

**Structure of the Local Bubble and Galactic Halo via  $O_{\text{VII}}$  and  $O_{\text{VIII}}$  emission lines in the direction of MBM20 and the Eridanus hole with XMM-Newton**

M. Galeazzi<sup>1</sup>, A. Gupta, K. Covey, and E. Ursino

Physics Department, University of Miami, Coral Gables, FL 33155

Received \_\_\_\_\_; accepted \_\_\_\_\_

arXiv:astro-ph/0609528v1 19 Sep 2006

---

<sup>1</sup>corresponding author, galeazzi@physics.miami.edu

## ABSTRACT

We analyzed two XMM-Newton observations in the direction of the high density, high latitude, neutral hydrogen cloud MBM20 and of a nearby low density region that we called the Eridanus hole. The cloud MBM20 is at a distance evaluated between 100 and 200 pc from the Sun and its density is sufficiently high to shield about 75% of the foreground emission in the 3/4 keV energy band. The combination of the two observations makes possible an evaluation of the O VII and O VIII emission both for the foreground component due to the Local Bubble, and the background one, due primary to the galactic halo. The two observations are in good agreement with each other and with ROSAT observations of the same part of the sky and the O VII and O VIII fluxes are  $O_{\text{VII}}=3.59\pm 0.56$  photons  $\text{cm}^{-2} \text{s}^{-1} \text{sr}^{-1}$ ,  $O_{\text{VIII}}=0.72\pm 0.24$  photons  $\text{cm}^{-2} \text{s}^{-1} \text{sr}^{-1}$  for MBM20 and  $O_{\text{VII}}=7.37 \pm 0.34$  photons  $\text{cm}^{-2} \text{s}^{-1} \text{sr}^{-1}$ ,  $O_{\text{VIII}}=1.73 \pm 0.17$  photons  $\text{cm}^{-2} \text{s}^{-1} \text{sr}^{-1}$  for the Eridanus hole. The spectra are in agreement with a simple three component model, one unabsorbed and one absorbed plasma component, and a power law, without evidence for any strong contamination from ion exchange in the solar system. Assuming that the two plasma components are in thermal equilibrium we obtain a temperature of 0.096 keV for the foreground component and 0.197 keV for the background one.

*Subject headings:* Local Bubble, Diffuse X-Ray background

## 1. Introduction

Optical and ultraviolet absorption line studies indicate that the Sun is located in a region of the interstellar medium of our Galaxy that is deficient in neutral matter, the Local

Cavity (Cox et al. 1987; Frisch et al. 1983; Bochkarev 1987). Observations of the X-ray background at energies below 1 keV indicate that this cavity is largely filled with million degree plasma, the Local Bubble (LB), and it extends for distances of the order of 100 pc in most directions.

Fits to data obtained with proportional counters have indicated temperatures near one million degrees for the LB, if one compares the shape of the pulse height distribution to predictions of models with normal solar abundances and collisional equilibrium ionization structure of the plasma (Snowden et al. 1998). Higher resolution spectral data over the 150-300 eV range obtained near the galactic plane with a Bragg crystal spectrometer (Sanders et al. 2001) confirm the thermal nature of the LB X-ray emission, but indicate that the above model picture is a bit naïve. The data suggest that the LB plasma is not in equilibrium and the abundances are probably not solar.

High resolution observations of the diffuse background at high galactic latitude obtained by ASCA in the 500-1000 eV range using CCD detectors (Gendreau et al. 1995) and by the XQC sounding rocket experiment in the 50-2000 eV range using microcalorimeter detectors (McCammon et al. 2002) detect the existence of the O VII and O VIII lines, but cannot separate the local bubble emission from galactic halo and extragalactic components. A more recent observation of the neutral hydrogen cloud MBM12 performed with Chandra (Smith et al. 2005), is also not able to clarify the picture as it seems affected by charge exchange within the solar system.

## 2. Observations

For this analysis we used two 100 ks observations taken with the XMM-Newton satellite in the direction respectively of the high density, high latitude, neutral hydrogen cloud

MBM20 and of a nearby low density region, that we called the Eridanus hole. MBM20 is a high latitude star forming cloud which is probably located within or at the edge of the Local Bubble. Its mass is  $84M_{\odot}$  and it is located at coordinates  $l=211^{\circ}23'53''.2, b=-36^{\circ}32'41''.8$ , southwest of the Orion star forming complex. The most recent evaluation of the distance  $d$  of MBM20 is based on interstellar NaI D absorption lines (Hearty et al. 2000). The nearest star which showed interstellar NaI D absorption in the line of sight to MBM20 is HD29851, at a distance of  $161 \pm 21$  pc using Hipparcos distances for stars. The farthest star which did not show NaI D absorption lines is HIP21508 at  $112 \pm 15$  pc. The currently accepted distance to MBM20 is therefore  $112 \pm 15$  pc  $< d < 161 \pm 21$  pc. The Eridanus hole, at coordinates  $l=213^{\circ}25'52''.3, b=-39^{\circ}5'26''.6$ , is a low neutral hydrogen region located about 2 degrees from the highest density part of MBM20.

We used the IRAS  $100 \mu\text{m}$  maps to evaluate the neutral hydrogen density in the two regions. The IRAS average brightness is  $13.34 \text{ MJy sr}^{-1}$ , and  $0.73 \text{ MJy sr}^{-1}$  for MBM20 and the Eridanus hole respectively. Using the "typical" high-latitude  $100 \mu\text{m}/N_{\text{H}}$  ratio of  $0.85 \times 10^{-20} \text{ cm}^2 \text{ MJy sr}^{-1}$  (Boulanger & Perault 1988) the evaluated neutral hydrogen densities are  $1.59 \times 10^{21} \text{ cm}^{-2}$  for MBM20 and  $0.86 \times 10^{20} \text{ cm}^{-2}$  for the Eridanus hole.

We can evaluate the shadow effect of MBM20 and the Eridanus hole in the 0.5-1 keV range, assuming that the background X-ray flux is due to thermal emission with  $\log_{10}(kT) = 6.2$ . We can then use the cross section calculated for the ROSAT R45 band as a good approximation of the cross section in the energy interval 0.5-1 keV. Using the calculation of Snowden et al. (1994) the cross section is approximately  $0.8 \times 10^{-21} \text{ cm}^2$  for MBM20 and  $1.0 \times 10^{-21} \text{ cm}^2$  for the Eridanus hole. We therefore expect that approximately 75% of the background in the MBM20 pointing is absorbed, while only about 8% of it is absorbed in the Eridanus hole pointing. The combination of the two observations allows good separation between foreground and background emission. Since MBM20 may be

outside the LB or fairly close to the LB wall in that direction (Sfeir et al. 1999), the separation should be roughly equivalent to a separation between Local Bubble and Galactic Halo emissions.

### 3. Data Analysis

Data from the full XMM-Newton field of view (approximately 30') were used in the analysis. The raw data were processed using the Standard Analysis Software (SAS)<sup>2</sup>. After a preliminary analysis we limited our interest only on the PN detector, since both the MOS1 and MOS2 presented a background noise too high. We selected events with pattern 0-4 (single+double) and flag equal to zero, to exclude bad pixels and CCD gaps. To remove the CCD pixels affected by proton flares and events above threshold, we generated light curves and removed all time intervals with a count rate greater than 20 counts s<sup>-1</sup>. Point sources were removed using our own code that iteratively identifies regions with count rate 3  $\sigma$  above the average observation count rate. After removal of bad pixels and point sources, the active field of view is  $5.0 \times 10^5$  sr for the MBM20 observation and  $4.9 \times 10^5$  sr for the Eridanus hole one.

#### 3.1. Background Removal

During the data analysis, we tried several procedures to properly evaluate the background. In the end we found that the relatively simple procedure reported here worked as well as any more complex one we tried. To account for systematic problems related to the background removal, a systematic error is included in our results. The systematic error

---

<sup>2</sup><http://xmm.vilspa.esa.es/sas/>

is evaluated by taking into account the spread in the results when different background removal procedures were used.

The non-cosmic background was modeled using a method similar to that proposed in Kuntz and Snowden (2004) and Read and Ponman (2003). The nominal non-cosmic background, which is dominated by the quiescent, high energy particle induced background, is modeled using closed-filter data (Read & Ponman 2003). To scale the closed-filter data to our observations, a spectrum of the closed filter dataset was created using the same procedure and filtering as was used to produce our spectra. The closed filter spectrum was then normalized using the counts in the Cu lines. We found that this procedure is very efficient at removing the "internal" background of the detector.

To remove the remaining ("external") background, we first subtracted from the spectra the well characterized power law component due to unidentified point sources (using the data from McCammon et al. 2002). Since this is the only significant component of the Diffuse X-ray Background (DXB) at high energy, the remaining spectrum at energies above about 2 keV is completely due to the external detector background. As can be seen in Fig. 1, above 2 keV this background is well described by a single exponential function of the energy both for MBM20 and the Eridanus hole data. To remove the external background from the region of our interest (0.5-1 keV), we then fit this exponential background above 2 keV and extend it, with the same parameters, in the region of interest. We then go back to our original data (after the internal background subtraction) and remove the exponential background to obtain the clean spectra. As will be discussed in the result section, the accuracy of the procedure has been confirmed by the good agreement between our data and ROSAT observations in the same directions. We also verified that the fitting range for the exponential background is not critical and small changes in the final result have been included in the systematic error.

#### 4. Analysis

A simple picture of the DXB nature points to the existence of three separate components, a local bubble component, modeled as an unabsorbed plasma thermal emission, a hotter galactic halo emission, modeled as a plasma thermal component absorbed by the gas in the galactic disk, and an unresolved extragalactic sources component (primarily AGNs), modeled as an absorbed power law. While high resolution observations in the 1/4 keV energy band have shown that this picture is too naïve (Sanders et al. 2001, McCammon et al. 2002), considering the energy resolution of the PN detector, we decided to use it as a starting point for our analysis. We used the XSPEC analysis package (Arnoud & Dormer 2002) to fit both spectra, in the energy range 0.4-2 keV, using a three component model. For plasma thermal emission the APEC model has been used <sup>3</sup>. In the fits, the neutral hydrogen density for the absorbed components was fixed to the average value obtained from the analysis of the IRAS-100 data ( $15.9 \times 10^{20} \text{ cm}^2$  and  $0.86 \times 10^{20} \text{ cm}^2$  for MBM20 and the Eridanus hole respectively), while all the other parameter were left free. A solar metal relative abundance has been chosen for the analysis (Anders et al. 1989). Due to a strong correlation between total metallicity and luminosity in the thermal components, we also decided to repeat the fits fixing the total metallicity to 1 (in solar units). The changes in the O VII and O VIII emission line fluxes due to different fitting procedures have been incorporate in the systematic error. In Table 1 we report the best fit parameters for the MBM20 and Eridanus hole datasets respectively, using a three components model, with fixed and free metal abundances.

In view of a reasonably good agreement between the fits of MBM20 and the Eridanus hole, we decided to fit both datasets at once, with a single set of parameters, except, of course, for the neutral hydrogen column density. The results are reported in Table 2, and

---

<sup>3</sup><http://hea-www.harvard.edu/APEC/>

the fits are shown in Fig. 2. In the table, the parameters obtained by McCammon et al. (2002) are also shown for comparison. The best fit results are in good agreement with those in McCammon et al. (2002), and the model fits very well the experimental data.

To verify the accuracy of our results, we folded our model with the ROSAT All Sky Survey (RASS) response matrix and calculated the expected count rate in the RASS 3/4 keV and 1.5 keV band and compared them with the measured RASS count rates in the direction of MBM20 and the Eridanus hole. The result is reported in Table 3 and shows good agreement between the two, giving us confidence in the accuracy of our data reduction and analysis. Having sufficient confidence in the fit results, we also used them to obtain the  $O_{\text{VII}}$  and  $O_{\text{VIII}}$  flux, which are reported in Table 4. In the table, the flux obtained by other investigations of the LB emission are also reported. As pointed out before, the error on the line flux is a combination of a purely statistical error and a systematic error that accounts for changes due to different analysis and background subtraction procedures.

Combining the MBM20 and Eridanus hole data we can evaluate  $O_{\text{VII}}$  and  $O_{\text{VIII}}$  emission of the foreground (LB) and background (galactic halo) components. Using the expression derived by Morrison and McCammon (1983), we find that MBM20 absorbs about 75% of the background  $O_{\text{VII}}$  emission and about 61% of the background  $O_{\text{VIII}}$  emission, while the Eridanus hole absorbs about 8% of the background  $O_{\text{VII}}$  emission and about 5% of the background  $O_{\text{VIII}}$  emission. Combining these data with our results, we evaluate the fluxes of  $O_{\text{VII}}$  and  $O_{\text{VIII}}$  for the foreground component (LB) as  $2.63 \pm 0.78$  photons  $\text{cm}^{-2} \text{s}^{-1} \text{sr}^{-1}$  and  $0.03 \pm 0.43$  photons  $\text{cm}^{-2} \text{s}^{-1} \text{sr}^{-1}$  respectively, and for the background component as  $5.03 \pm 0.98$  photons  $\text{cm}^{-2} \text{s}^{-1} \text{sr}^{-1}$  and  $1.68 \pm 0.53$  photons  $\text{cm}^{-2} \text{s}^{-1} \text{sr}^{-1}$ .

Our results are significantly different from what has been found in a Chandra observation of the neutral hydrogen cloud MBM12, where a very strong  $O_{\text{VIII}}$  emission line was observed (Smith et al. 2005) and the simple three component model could not be

used successfully. The authors of the MBM12 paper concluded that their measurement was probably affected by particularly strong emission due to charge exchange within the solar system. Assuming that the higher O VIII emission is, in fact, a signature of charge exchange within the solar system, we can conclude that such contamination is not significant in our data.

We investigated the possibility that the discrepancy with the MBM12 data could be purely due to a different pointing directions. We used the maps of the expected X-ray emission due to charge exchange with interstellar neutrals and geocoronal hydrogen within the solar system generated by Robertson and Cravens (2003) to evaluate the expected contribution in the direction of MBM20 and MBM12. From the X-ray map at the time of the ROSAT 1990-1991 sky survey, we find that the X-ray intensity due to charge exchange in MBM12 is  $4\text{-}5 \text{ keV cm}^{-2} \text{ s}^{-1} \text{ sr}^{-1}$ , while in the MBM20 direction is  $3\text{-}4 \text{ keV cm}^{-2} \text{ s}^{-1} \text{ sr}^{-1}$ . While, in fact, the emission in the direction of MBM20 is expected to be smaller, the difference should be less than 30%, which cannot explain the difference between our results and those of Smith et al. (2005). We should therefore conclude that either the high O VIII emission in the MBM12 observation is of different nature, or it is affected by a strong transient component which is not present in the MBM20 and Eridanus hole data.

## 5. Conclusions

In studying the Diffuse X-ray Background (DXB), a challenging task is the separation between the different components contributing to it. This is particularly difficult due to the low DXB flux compared to the relatively high detector background. The contemporary study of a high latitude, high density cloud and a low density region nearby has proven an effective tool for the separation of foreground and background components. In our investigation we found a simple, efficient method to evaluate the detector background and

the comparison of the two pointing gives us good separation between the two main DXB components, i.e., Local Bubble and galactic halo. The results are consistent with a simple three components model of the DXB: an unabsorbed plasma component with temperature of 0.096 keV, an absorbed plasma component with temperature of 0.197 keV, and a power law, without evidence for any strong contamination from ion exchange in the solar system.

We would like to thank Kip Kuntz for the useful discussion about XMM-Newton background removal and for providing us preprints of his publication on the subject. We would also like to thank Wilt Sanders for the useful discussion and suggestions.

## REFERENCES

- Anders, E., et al., 1989, *Geochimica et Cosmochimica Acta*, 53, 197
- Arnaud, K. & Dormer, B. 2002, XSPEC: An X-Ray Spectral Fitting package, User's Guide for version 11.2.x, HEASARC, Exploration of the Universe Division, NASA/GSFC, Greenbelt, MD 20771, <http://heasarc.gsfc.nasa.gov/docs/xanadu/xspec/manual/manual.html>
- Bochkarev, N. G. et al. 1987, *Soviet Ast.*, 31, 20
- Boulangier, F., and Perault, M. 1988, *ApJ*, 330, 964
- Cox, D. P., et al. 1987, *ARA&A*, 25, 303
- Frisch, P. L., et al. 1983, *ApJ*, 271, 59
- Gendreau, K. C., et al. 1995, *PASJ*, 47, L5
- Hearty, T., et al. 2000, *A&A*, 357, 681
- McCammon, D., et al. 2002, *ApJ*, 576, 188
- Morrison, R. & McCammon, D., et al. 1983, *ApJ*, 270, 119
- Read, A. M. & Ponman, T. J. 2003, *A&A*, 409, 395
- Robertson, I. P. & Cravens, T. E. 2003, *J. Geophys. Res.*, 108, A10, LIS 6-1
- Sanders, W. T., et al. 2001, *ApJ*, 554, 694
- Sfeir, D. M., et al. 1999, *A&A*, 346, 785
- Smith, R. K., et al., 2005, *ApJ*, 623, 225
- Snowden, S. L., et al., 1994, *ApJ*, 424, 714

Snowden, S. L., et al., 1998, ApJ, 493, 715

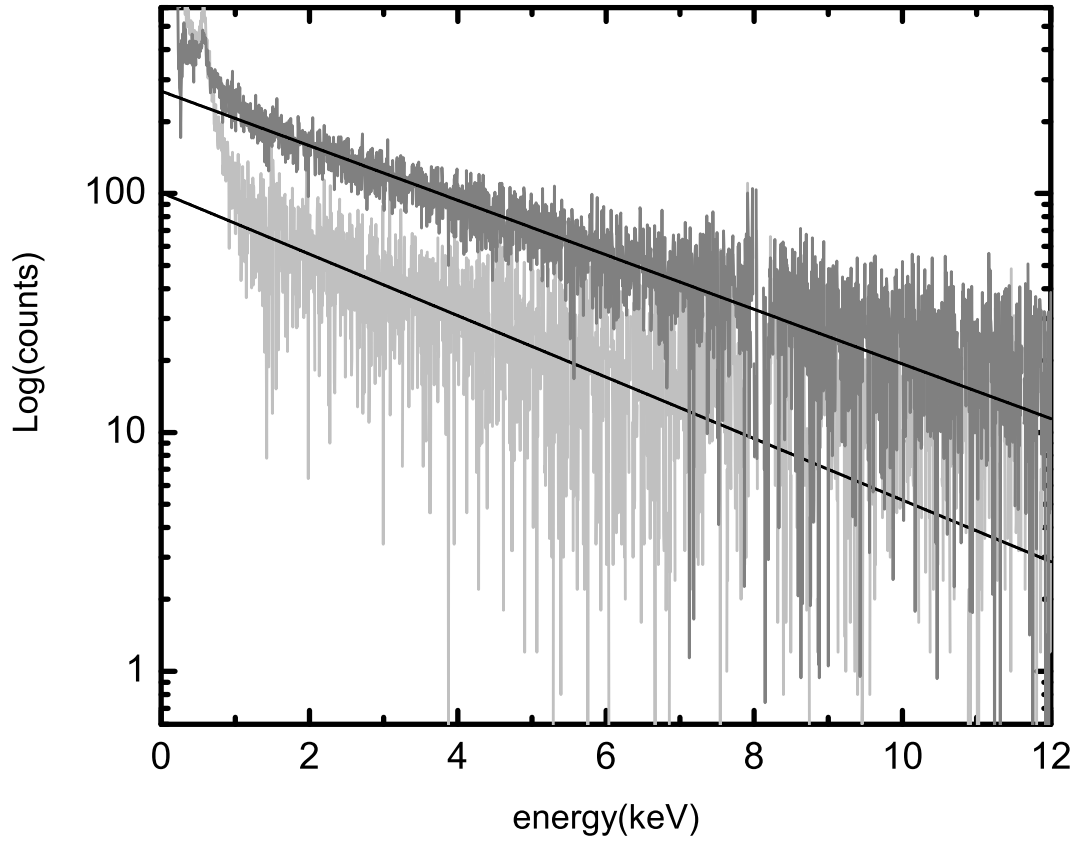


Fig. 1.— Energy spectrum from the MBM20 (dark grey line) and Eridanus hole (grey line) observations after subtracting the internal background and the unidentified sources component. The events above about 2 keV are completely due to external detector background and can be well characterized by a simple exponential function of the energy.

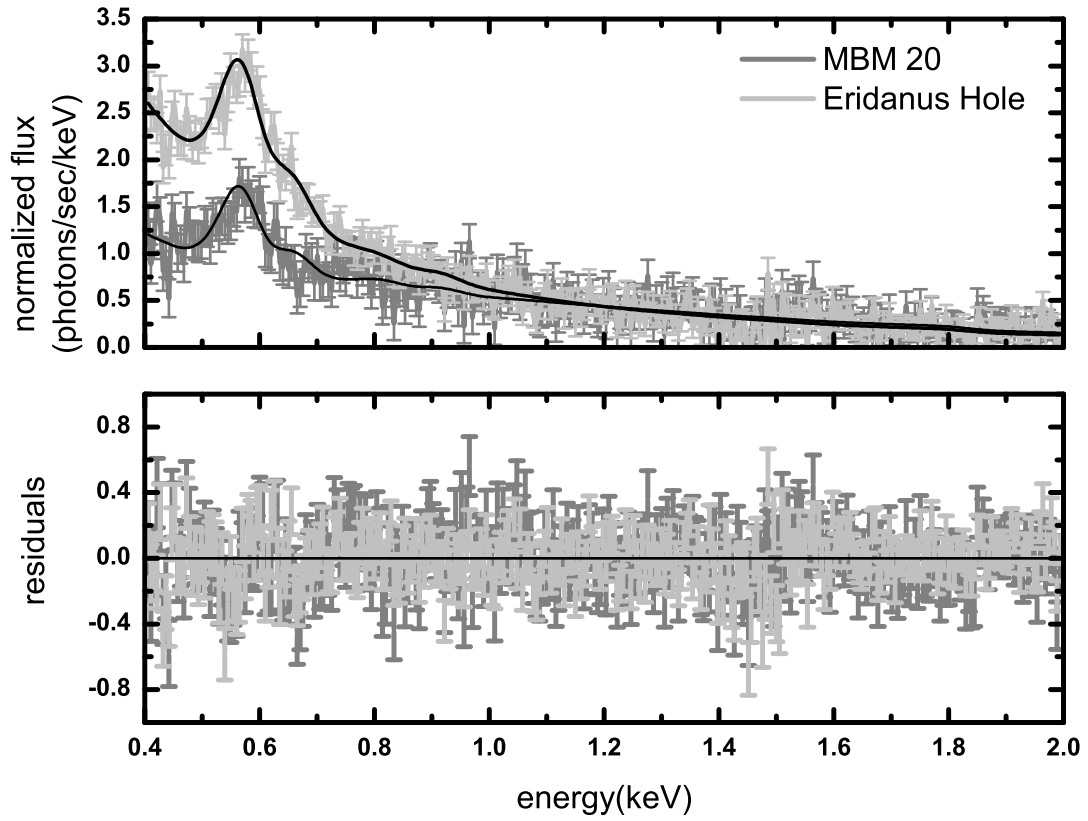


Fig. 2.— Global fit for MBM20 and Eridanus hole data. The datapoints represent the experimental data, the black lines the best fits.

Table 1. Best fit parameters for the MBM20 and Eridanus hole datasets respectively, using a three components model. The terms "Free" and "Frozen" refers to Free abundance and Frozen abundance.

	Units	MBM20		Eridanus hole	
		Free	Frozen	Free	Frozen
<b>Unabsorbed plasma</b>					
<b>component:</b>					
Temperature	keV	0.114	0.099	0.097	0.094
	K	$1.33 \times 10^6$	$1.15 \times 10^6$	$1.13 \times 10^6$	$1.09 \times 10^6$
Abundance	Solar Units	0.92	1	0.54	1
Redshift		0	0	0	0
Normalization		$5.32 \times 10^{-4}$	$8.5 \times 10^{-4}$	$2.2 \times 10^{-3}$	$1.34 \times 10^{-3}$
<b>Absorbed plasma</b>					
<b>component:</b>					
nH	$10^{22} \text{ cm}^2$	0.159	0.159	0.0086	0.0086
Temperature	keV	0.21	0.242	0.211	0.205
	K	$2.44 \times 10^6$	$2.81 \times 10^6$	$2.45 \times 10^6$	$2.38 \times 10^6$
Abundance	Solar Units	0.667	1	0.208	1
Redshift		0	0	0	0
Normalization		$1.02 \times 10^{-4}$	$1.53 \times 10^{-4}$	$1.2 \times 10^{-3}$	$2.77 \times 10^{-3}$
<b>Absorbed power law:</b>					
Photon Index		2.48	2.32	1.93	1.99
Normalization		$8.08 \times 10^{-4}$	$7.58 \times 10^{-4}$	$6.22 \times 10^{-4}$	$6.3 \times 10^{-4}$

Table 1—Continued

---

---

	<u>MBM20</u>		<u>Eridanus hole</u>	
Units	Free	Frozen	Free	Frozen

---

---

Table 2. Model Parameters for global fit of MBM20 and Eridanus hole data. In the neutral hydrogen density, the first value refers to the MBM20 observation, the second to the Eridanus hole one. The Normalization terms in the data from McCammon et al. (2002) are scaled to the FOV of our observations ( $5.0 \times 10^{-5}$  sr).

	Units	Free Abundance	Frozen Abundance	McCammon(2002)
<b>Unabsorbed plasma</b>				
<b>component:</b>				
Temperature	keV	0.104	0.096	0.099
	K	$1.2 \times 10^6$	$1.11 \times 10^6$	$1.15 \times 10^6$
Abundance	Solar Units	0.39	1	1
Redshift		0	0	0
Normalization		$3.56 \times 10^{-3}$	$9.34 \times 10^{-4}$	$9.10 \times 10^{-4}$
<b>Absorbed plasma</b>				
<b>component:</b>				
nH	$10^{22}$ cm <sup>2</sup>	0.159/0.0086	0.159/0.0086	
Temperature	keV	0.196	0.197	0.225
	K	$2.19 \times 10^6$	$2.27 \times 10^6$	$2.62 \times 10^6$
Abundance	Solar Units	0.453	1	1
Redshift		0	0	0
Normalization		$8.41 \times 10^{-4}$	$3.15 \times 10^{-4}$	$3.80 \times 10^{-4}$
<b>Absorbed power law:</b>				
Photon Index		2.12	2.14	1.52
Normalization		$7.39 \times 10^{-4}$	$7.09 \times 10^{-4}$	$6.34 \times 10^{-4}$

Table 3. Fluxes in Equivalent ROSAT bands. The "XMM" data represent the fluxes obtained using our best fit parameters folded through the ROSAT response function. The "ROSAT" data are ROSAT measured fluxes in the same direction. The units are  $10^{-6}$  counts  $s^{-1}$  arcmin $^{-2}$ .

	MBM20		Eridanus hole	
ROSAT BAND	XMM	ROSAT	XMM	ROSAT
R45	71	$71 \pm 20$	139.3	$130 \pm 26$
R67	100.1	$98 \pm 19$	131.7	$124 \pm 18$

Table 4. O<sub>VII</sub> and O<sub>VIII</sub> emission compared with previous estimates

Experiment	N <sub>H</sub> (10 <sup>20</sup> atoms cm <sup>-2</sup> )	O <sub>VII</sub> (ph s <sup>-1</sup> cm <sup>2</sup> sr <sup>-1</sup> )	O <sub>VIII</sub> (ph s <sup>-1</sup> cm <sup>2</sup> sr <sup>-1</sup> )
MBM20	15.9	3.59 ± 0.56	0.72 ± 0.24
Eridanus hole	0.86	7.37 ± 0.34	1.73 ± 0.17
Smith et al. 2005	40	1.79 ± 0.55	2.34 ± 0.36
Gendreau et al. 1995	6	2.3 ± 0.3	0.6 ± 0.15
McCammon et al. 2002	1.8	4.8 ± 0.8	1.6 ± 0.4